

Phase Crossover induced by Dynamical Many Body Localization in Periodically Driven Long-Range Spin Systems

Mahbub Rahaman,¹ Takashi Mori,² and Analabha Roy¹

¹Department of Physics, The University of Burdwan, Golapbag, Bardhaman - 713 104, India

²RIKEN CEMS, 2-1 Hirosawa, Wako, Saitama, 351-0198, Japan

Dynamical many-body freezing occurs in periodic transverse field-driven integrable quantum spin systems. Under resonance conditions, quantum dynamics causes practically infinite hysteresis in the drive response, maintaining its starting value. We extended this to non-integrable many body systems by reducing the Hamiltonian symmetries through a power-law dependence in spin exchange energy, $J_{ij} = 1/|i - j|^\beta$. The dynamics of the integrable short-range Transverse Field Ising Model (TFIM) and non-integrable long-range Lipkin Meshkov-Glick (LMG) models were investigated. In the LMG, the resonance conditions in the driving field suppresses the heating postulated by the *Eigenstate Thermalization Hypothesis* (ETH) by inducing *Dynamical Many Body Localization*, or DMBL. This is in contrast to Many Body Localization (MBL), which requires disorder to suppress ETH. DMBL has been validated by the Inverse Participation Ratio (IPR) of the quasi-stationary Floquet modes. While TFIM has IPR localization for all drive parameters, the LMG exhibits high-frequency localization only at the resonances. IPR localization in the LMG deteriorates with an inverse system size law at lower frequencies, which indicates heating to infinite temperature. Furthermore, adiabatically increasing frequency and amplitude from low values raises the Floquet state IPR in the LMG from nearly zero to unity, indicating a phase crossover. This occurrence enables a future technique to construct an MBL engine in clean systems that can be cycled by adjusting drive parameters only.

Keywords: Dynamical localization, Thermalization, Phase Crossover

Under certain resonance conditions in the drive parameters, periodically driven quantum many-body systems can experience dynamical many-body freezing (DMF), which causes the response to freeze completely to its initial value at all times [1–3]. This arises as a consequence of additional approximate symmetries that occur at resonance. DMF has been demonstrated via the Rotating Wave Approximation (RWA) in the driven TFIM with nearest-neighbour interactions [4] and is shown to be protected when translational invariance is explicitly broken (say, by disorder) [5, 6].

The utilization of Floquet theory simplifies the analysis of time-periodic systems. For closed quantum systems governed by the time-dependent Schrödinger equation, the *Floquet Hamiltonian* allows for a mapping of the time-dependent dynamics into the dynamics of a time-independent effective Hamiltonian, provided the system is strobed at integer multiples of the time period of the drive. The time independent eigenstates of the effective Hamiltonian correspond to quasi-stationary *Floquet Modes* of the original Hamiltonian. The temporal progression of the system comes from phase coefficients that capture the dynamics [7, 8].

Any sufficiently complex non-integrable Many Body System is expected to thermalize according to the Eigenstate Thermalization Hypothesis (ETH) despite the fact that closed quantum dynamics preserves the memory of the initial state of the system. This arises due to the properties of the matrix elements of ob-

servables in typical states[9]. The ETH can be readily adapted to time-periodic systems using Floquet theory (the Floquet-ETH, or FETH). Nonetheless, the conditions for ETH to hold are not particularly strong, and the density matrix of the system can fail to approach one that is described by a thermal expression. Thermal systems must conduct because they exchange energy and particles internally during thermalization. Thus, insulating systems can be naturally athermal; Many Body Localization (MBL) is a well-studied case [10]. This phenomenon is stable against local perturbations, and constitutes an exotic state of matter with far-reaching implications in theoretical physics, as well as in practical applications[11].

The addition of disorder has been identified as a crucial component in the onset of MBL. In that case, thermalization is prevented by disorder-induced localization. Nonetheless, alternative approaches to MBL in strongly interacting disorder-free systems [12–14], inhomogeneous systems [15–18], and by inducing disorder in the emergent physics [19] and by other effective means [17] (albeit with strong finite-size effects), have been reported. An alternative approach to realizing MBL in disorder-free *homogeneous* many-body systems involve *Floquet Engineering*, where a time-periodic drive is introduced, and the drive parameters tuned to introduce a clustering of quasistationary energies in a manner similar to localization[9].

In this article, we use the fact that emergent approximate symmetries can be engineered in Floquet

systems and apply it to long-range interactions This
 results in *Dynamical Many Body Localization* (DMBL)
 at resonant values of the drive parameters, and com-
 plete thermal behaviour at other values. This phe-
 nomenon is distinct from DMF in the TFIM, since
 clean TFIM systems, being integrable, never thermal-
 ize.

To demonstrate the onset of MBL, we investigate
 the driven Lipkin-Meshkov-Glick (LMG) model[20–
 25], a long-range system that extends the nearest-
 neighbour interactions in the TFIM to all-to-all inter-
 actions. [26–28] We have recovered the onset of DMF
 in this system and have supported our result with nu-
 merical simulations.

In addition, we compare the degree of localization
 of the quasi-stationary Floquet modes in the LMG
 model with the TFIM. In order to do so, we look at the
 Inverse Participation Ratio (IPR) of the Floquet modes
 in the representation given by the eigenstates of the
 symmetry-breaking field. The IPR, closely related to
 the concept of quantum purity, is defined as the formal
 sum of the square of the density in some physically
 meaningful space or representation. A high IPR of a
 stationary state denotes low participation in most of
 the representation, and a low IPR distributes partic-
 ipation uniformly across the representation, leading
 to ergodic dynamics[29]. Thus, IPR [30] is a useful
 tool for witnessing MBL of a quantum system. For an
 MBL system, the IPR is unity, and it scales inversely
 with the number of spins when it is thermally dis-
 tributed [31].

In the first section of this paper, we present all es-
 sential theoretical frameworks. Our results for the
 LMG model are presented next in section II. In that
 section, we have used the Rotating Wave Approx-
 imation (RWA) [32], where only the slowest rotating
 terms in the Fourier expansion of the Hamiltonian in
 a frame co-rotating with the symmetry breaking drive
 field are retained. In addition, we have the obtained
 numerical simulations of the Floquet modes and their
 IPR. They are used to probe the system dynamics in
 the high and low-frequency domains at both limits of
 β . In section III we have used phase space plots to
 contrast the low and high frequency limits of the LMG
 model in the thermodynamic limit by mapping it to an
 equivalent classical Hamiltonian system. Finally, in
 section IV, we have looked at numerical computations
 of the IPR of the Floquet modes for different values of
 the drive parameters, well beyond those that allow for
 the RWA. We observed that, if the system is driven by
 an adiabatically increasing drive frequency from low
 to high limit while remaining in the resonance region,
 a sharp crossover from a thermal to an MBL phase
 occurs. We conclude with discussions and outlook.

I. BACKGROUND

The Eigenstate Thermalization Hypothesis (ETH) is
 a series of conjectures that allows for the thermaliza-
 tion of an isolated quantum many body system. The
 state of the system, $|\psi(t)\rangle$, evolves according to the
 Schrödinger equation $\hat{H}|\psi(t)\rangle = i\frac{\partial}{\partial t}|\psi\rangle$. The Hamilto-
 nian \hat{H} is assumed to be *non-integrable*, in that it lacks
 an extensive number of conserved quantities that can
 be written as a sum of local operators, that is to say,
 there are no set of observables $\hat{O}_s = \sum_i \hat{L}_i$ such that
 $[\hat{O}_s, \hat{H}] = 0$. Here, the \hat{O}_s constitute an arbitrary
 CSCO (complete set of commuting observables), and
 \hat{L}_i are *local*, each having sub-extensive support in the
 system [33]. In addition, we postulate an "equilib-
 rium" value A_{eq} for every observable \hat{A} , such that

$$A_{eq}(E) \equiv \frac{\text{Tr}(\hat{A}e^{-\beta\hat{H}})}{\text{Tr}(e^{-\beta\hat{H}})}, \quad (1)$$

where $E = \langle\psi(t)|\hat{H}|\psi(t)\rangle$ is the conserved energy of
 the system, and $\beta = 1/(k_B T)$ is the inverse tempera-
 ture, H_{eq} is an effective Hamiltonian that captures the
 long-time average dynamics of the system, and k_B is
 the Boltzmann constant.

To put it simply, ETH proposes that this many-
 body Hamiltonian undergoes thermalization as seen
 in the *long-time averages* of observables, with the
 eigenstates bearing resemblance to thermal states.
 The aforementioned hypothesis serves as a valuable
 instrument for comprehending the conduct of stim-
 ulated quantum systems and their correlation with
 thermal equilibrium. This assertion can be justified
 by examining the expectation value of an observable
 \hat{A} as it evolves under the Schrödinger equation. To
 see this, we first expand the state of the system $|\psi(t)\rangle$
 as:

$$|\psi(t)\rangle = \sum_m c_m(t) |m(0)\rangle,$$

where $|m(0)\rangle$ represents the eigenstates of $\hat{H}(0)$ with
 energy E_m . The coefficients $c_m(t)$ describe the time-
 dependent amplitude of the expansion. Plugging
 these expansions into the expression for the expec-
 tation value, we obtain the long-time average of the
 expectation value [34]:

$$\overline{\langle \hat{A}(t) \rangle} = \sum_{m,k} \overline{c_m^*(t)c_k(t)} \langle m(0)|\hat{A}|k(0)\rangle, \quad (2)$$

where the overline indicates the following operation
 for any time-dependent quantity $\mathcal{O}(t)$,

$$\overline{\mathcal{O}} \equiv \lim_{t \rightarrow \infty} \frac{1}{t} \int_0^t d\tau \mathcal{O}(\tau). \quad (3)$$

The matrix elements $\langle m(0)|\hat{A}|k(0)\rangle$ are said to satisfy the Srednicki ansatz [35, 36]:

$$\begin{aligned} \langle m(0)|\hat{A}|k(0)\rangle &\approx A_{eq} \left(\frac{E_m + E_k}{2} \right) \delta_{mk} + \\ &e^{-\frac{1}{2}S\left(\frac{E_m+E_k}{2}\right)} f\left(\frac{E_m + E_k}{2}, E_m - E_k\right) R_{mk}. \end{aligned} \quad (4)$$

Here, S is the thermodynamic entropy and R_{mk} are elements of a random matrix with vanishing mean and unit variance. What this means for the ensuing dynamics is that the system explores the accessible Hilbert space uniformly, and the matrix elements $\langle m(0)|\hat{A}(t)|k(0)\rangle$ become indistinguishable for most pairs of m and k . Applying this ansatz and taking the thermodynamic limit by ignoring terms $\mathcal{O}(e^{-S/2})$, the expression for the expectation value becomes:

$$\begin{aligned} \overline{\langle \hat{A}(t) \rangle} &\approx \sum_m \overline{|c_m(t)|^2} A_{eq}(E_m) \\ &\approx A_{eq}(E) \sum_m \overline{|c_m(t)|^2} = A_{eq}(E), \end{aligned}$$

where, in the last step, we utilized the fact that A_{eq} is a smooth function, and that the states with energies far from E have $|c_m(t)|^2 \approx 0$. Therefore, in the limit of large systems the expectation value of an observable \hat{A} is approximately equal to the thermal expectation value A_{eq} . This is the essence of the ETH, which suggests that individual eigenstates of a quantum system can be described by statistical mechanics in the long-time limit.

We now generalize the ETH to non-integrable many body systems that are closed, but not isolated. In that case, it is possible to impart a periodic time-dependence on the Hamiltonian while still ensuring unitary evolution. If the time period of the drive is T , and the corresponding drive frequency $\omega \equiv 2\pi/T$, the Floquet theorem states that the solutions to the Schrödinger equation can be written as $|\psi(t)\rangle = e^{-i\epsilon t/\hbar} |\phi(t)\rangle$, where the $|\phi(t)\rangle$ are T -periodic states called *Floquet Modes*, the corresponding $\epsilon \in \mathbb{R}$, are called *quasienergies*. Quasienergy values are not unique, and can be made to be bounded within a Floquet Brillouin zone, viz. a range $[-\omega/2, \omega/2]$ [37, 38]. As a consequence, the unitary evolution operator can be split into two parts as follows [39].

$$U(t) = e^{-i\hat{K}_F(t)} e^{-i\hat{H}_F t}. \quad (5)$$

Here, the micromotion operator $\hat{K}_F(t)$ is time-periodic in T , with $\hat{K}_F(0) = 0$, and the Floquet Hamiltonian $\hat{H}_F = e^{i\hat{K}_F(t)} [\hat{H}(t) - i\partial_t] e^{-i\hat{K}_F(t)}$. Thus, if the system is strobed at integer multiples of T only, then the unitary evolution matches that of a time independent Hamiltonian H_F . This can capture most of

the exact dynamics at large frequencies. In such systems, the *Floquet Eigenstate Thermalization Hypothesis* (FETH) posits that, subject to specific conditions and in the context of a system of significant size, the Floquet modes themselves exhibit thermal state-like behavior, i.e., $\hat{H} \approx \hat{H}_F$ in eqn 1. However, in contrast to the isolated systems, the loss of energy conservation allows for the mixing of all Floquet modes in the ensuing dynamics, not just those with quasienergies near E . Were this to actually happen in the ensuing dynamics, it can be reconciled with ETH by ensuring that the RHS of eqn 1 is independent of β , i.e., an infinite temperature ensemble [40]. In other words, the nonequilibrium steady state of the system tends to an infinite temperature, maximum entropy density matrix.

However, drive parameters like amplitude, frequency, and duty-cycle strongly affect the structure of the Floquet modes $|\phi\rangle$. Thus, they can be engineered to prevent the kind of full mixing that would lead to infinite temperatures, manifesting suppression of thermalization dynamically. Thus, this type of *Floquet Engineering* can produce *Dynamical Many Body Localization* (DMBL), where the system fails to reach thermal equilibrium and remains localized, possibly near its initial state, even at large times. This paradigm seems similar to standard Many-Body Localization [41, 42], where disorder, locality, and integrability can cause athermality via breakdown in the Srednicki ansatz. However, DMBL stems from periodic driving, and thus can occur regardless of disorder, locality of observables, or system integrability, all of which have been studied for MBL onset [41, 43, 44].

Integrable Many Body systems do not exhibit thermalization. When subjected to time-periodic drives, Floquet engineering allows for the introduction of additional approximate conserved quantities that dynamically suppress the evolution of certain observables by hysteresis. This type of *freezing* of response has been shown in integrable systems [6]. A paradigmatic example is the driven Transverse Field Ising model (TFIM) in one dimension [45]. The Hamiltonian is given by

$$\hat{H}(t) = \hat{H}_0 + h_z(t) \hat{H}_1, \quad (6)$$

$$\hat{H}_0 = -\frac{1}{2} \sum_{i=1}^N \sigma_i^x \sigma_{i+1}^x, \quad (7)$$

$$\hat{H}_1 = -\frac{1}{2} \sum_{i=1}^N \sigma_i^z. \quad (8)$$

Here, the undriven Hamiltonian \hat{H}_0 consists of nearest-neighbour interactions between N number of spin-1/2 particles on a one-dimensional spin network. The transverse field is denoted by \hat{H}_1 , and is

being varied by a time-periodic and harmonic signal $h_z(t) = h_0 + h \cos \omega t$, yielding a time period $T = 2\pi/\omega$ with amplitude h , drive frequency ω , and d.c. field h_0 . This Hamiltonian can be readily transformed into a spinless pseudo-fermionic system via the Jordan-Wigner transformation [4]. When written in momentum space spanned by spinors $\psi_k = (c_{-k}, c_k^\dagger)^T$ of fermions at momentum k created (annihilated) by operators c_k^\dagger (c_k), the effective Hamiltonian

$$H(t) = \sum_{(k, -k)-\text{pairs}} \psi_k^\dagger \left[\left(f_k - h_z(t) \right) \tau_z + \tau_x \Delta_k \right] \psi_k, \quad (9)$$

where $f_k = \cos k$, $\Delta_k = \sin k$, τ_{xyz} are the three Pauli Matrices, and the sum is over distinct $(k, -k)$ Cooper Pairs. We can transform our system to a frame that rotates with the time-varying symmetry-breaking field. This is achieved by the means of the unitary transformation operator

$$\begin{aligned} U(t) &= \prod_k U_k(t) \\ U_k(t) &= \exp \left\{ \left[\frac{i\hbar}{\omega} \sin \omega t \right] \tau_z \right\}. \end{aligned} \quad (10)$$

The resulting transformed Hamiltonian $H'(t) = U^\dagger(t) H(t) U(t) - iU^\dagger(t) \partial_t U(t)$ simplifies to

$$\begin{aligned} H'(t) &= \sum_{(k, -k)-\text{pairs}} \psi_k^\dagger \left[\tau_z f_k + \tau_x \cos(\eta \sin \omega t) \right. \\ &\quad \left. + \tau_y \sin(\eta \sin \omega t) \right] \psi_k, \end{aligned} \quad (11)$$

where we defined $\eta = 2h/\omega$. Using the Jacobi-Anger formula [46]

$$e^{i\eta \sin \omega t} = \sum_{n=-\infty}^{\infty} J_n(\eta) e^{in\omega t}, \quad (12)$$

where $J_n(\eta)$ are Bessel Functions, the transformed Hamiltonian simplifies to

$$\begin{aligned} H'(t) &= \sum_{(k, -k)-\text{pairs}} \psi_k^\dagger \left\{ \tau_z f_k + 2\tau_x \Delta_k \sum_{n \geq 0} J_{2n}(\eta) \cos(2n\omega t) \right. \\ &\quad \left. - 2\tau_y \Delta_k \sum_{n \geq 0} J_{2n+1}(\eta) \sin[(2n+1)\omega t] \right\} \psi_k. \end{aligned} \quad (13)$$

In the frequency regime $\omega \gg f_k$, the long-time average $H^{RWA} \equiv \lim_{n \rightarrow \infty} \frac{1}{nT} \int_0^{nT} dt H'(t)$ can serve as a suitable approximation for $H'(t)$. This approximation,

known as the *Rotated Wave Approximation* (RWA), eliminates the oscillating modes and results in an effective Hamiltonian that is independent of time,

$$H^{RWA} = \sum_{(k, -k)-\text{pairs}} \psi_k^\dagger \left[f_k \tau_z + 2J_0(\eta) \Delta_k \tau_x \right] \psi_k. \quad (14)$$

It is evident that by manipulating the drive parameters, specifically the amplitude denoted by h and the frequency denoted by ω , in a manner such that η is positioned on a root of $J_0(\eta)$, the fermion number can be conserved to a significant extent at this particular resonance. Consequently, it is feasible to exercise direct control over H^{RWA} , resulting in a comprehensive suppression of the dynamics of otherwise responsive observables.

This phenomenon is highly general in nature, and can be readily adapted to non-integrable systems. In such cases, freezing has the additional effect of inducing DMBL, suppressing thermalization to infinite temperatures. Numerical quantification of localization of a specific (quasi) stationary state in a physically significant representation can be achieved through the computation of the *Inverse Participation Ratio* (IPR). The IPR is generally defined as the formal sum over the square of the local density in a physically meaningful space. [47–50] In the single particle case, the IPR, for a state $|\psi\rangle$ can be written as

$$\phi_{IPR} \equiv \int dx |\langle x | \psi \rangle|^4.$$

This definition can be applied to obtain the IPR of a state $|\phi\rangle$ in a representation given by any single particle basis $|m\rangle$ as

$$\phi_{IPR} \equiv \sum_m |\langle m | \psi \rangle|^4. \quad (15)$$

The smallest value of the IPR corresponds to a fully de-localized state, $\psi(x) = 1/\sqrt{N}$ for a system of size N [50, 51]. Values of the IPR close to unity correspond to localized states [30]. For a periodically driven system, we look at the IPR of the quasi-stationary Floquet modes at $t = T$, where $t = 2\pi/\omega$ for drive frequency ω . In the TFIM model, equation 14 indicates that, at resonance, when $J_0(\eta) = 0$, the Floquet modes are approximately given by the fermionic Fock states, which have a trivially unit IPR in the representation of the eigenmodes of the transverse field \hat{H}_1 in equation 6. Here, a particular Floquet mode can be decomposed into a direct product of cooper-pair states as $|\phi\rangle = \prod_{k, -k} |\phi_k^n\rangle$. In the RWA limit and at resonance, $|\phi_k^n\rangle$ has values of $|0\rangle, |k, -k\rangle$ for two values of $n = 0, 1$ respectively. We define the reduced IPR of $|\phi_k^n\rangle \forall k$ to be

$$\phi_{IPR}^{(n)}(k) = |\langle 0 | \phi_k^n \rangle|^4 + |\langle +k, -k | \phi_k^n \rangle|^4, \quad (16)$$

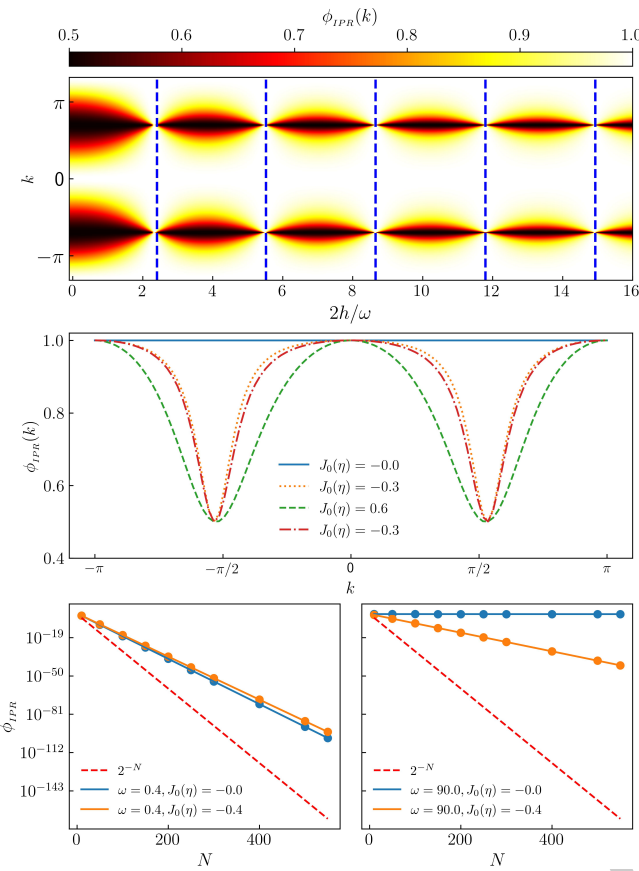


FIG. 1. Reduced IPR (defined in equation 16) for one of the two Floquet modes obtained from the exact dynamics of the TFIM for size $N = 100$, $\omega = 90$ for the entire Brillouin zone (top panel, ordinate) and a few drive amplitudes (top panel, abscissa). The dashed lines (top panel) indicate the roots of $J_0(\eta)$. The middle panel shows cross-sections of the reduced IPR in k -space for four chosen amplitudes. Finally, the bottom panels show semi-log plots of the scaling with N of the full many body IPR as defined in eqn 17, with the left panel for a small $\omega = 0.4$, amplitude h chosen to lie both in and out of the root of $J_0(\eta)$ as indicated in the legend, with similar plots on the right panel for a large $\omega = 90$.

where $n = 0, 1$. The full many-body IPR can be obtained from the reduced IPR in eqn 16 by a product over all momenta in the Brillouin zone, yielding

$$\phi_{IPR} = \prod_k \phi_{IPR}^{(n)}(k). \quad (17)$$

In the RWA limit and at resonance, this quantity is unity, indicating very low participation and the onset of freezing. Figure 1 shows results from numerically simulating the TFIM dynamics. The reduced IPR for a particular Floquet mode recovered by simulating the exact Schrödinger dynamics over a single time period of the drive, and plotted as a function of momentum k for different η 's. At resonance, when η lies at the root of the Bessel function $J_0(\eta)$, the Reduced IPR is nearly

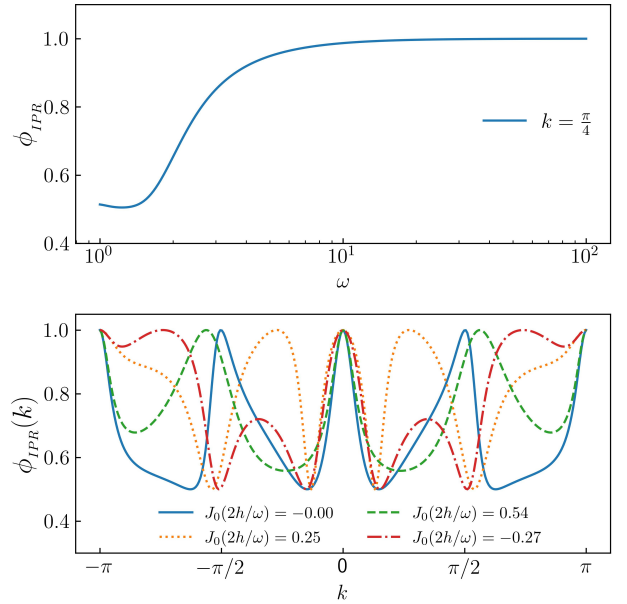


FIG. 2. Reduced IPR obtained by adiabatically increasing ω (top panel abscissa) for one the floquet mode obtained from equation 16 at the root of $J_0(\eta)$ for $N = 500$. IPR is ~ 0.5 (localized yet not fully freezing) upto $\omega \sim 2$, after that, smoothly increased to unity (fully localized and freezing) at higher $\omega \geq 10$ (top panel, ordinate). At bottom panel cross-sections for four chosen amplitudes at $\omega = 2$ are plotted for a brillouin zone (abscissa) with corresponding reduced IPRs (ordinate).

unity for all momenta. Consequently, so is ϕ_{IPR} . Outside this resonance, the IPR is unity only for some momenta because the effective Hamiltonian is perfectly diagonal at $k \in \{-\pi, 0, \pi\}$ as can be seen in the cross-sectional plots of figure 1. As we move away from the resonance point, the full IPR decreases exponentially as a power law in the system size, as can be seen in the bottom-right panel of fig 2. However, as the TFIM is an integrable spin model, the IPR never drops to a value that is small enough to indicate thermalization. This can be seen in the bottom panels of figure 2, where the power-law decay of $\phi_{IPR}(N)$ never approaches the thermodynamic scaling law $\phi_{IPR}(N) \sim 2^{-N}$ for either small or large frequencies. Note that, at low frequencies, RWA complete localization fails due to the unavailability of zero off-diagonal terms in the effective transformed Hamiltonian, as well as the absence of integrability breaking terms to counteract the off diagonal terms. Because the TFIM can be mapped to a system of noninteracting particles as shown in eqn 9, it is not physically meaningful to refer to the unit IPR region as "Many Body Localization", because the parameter space lacks a thermalized region to contrast with this state. The type of Floquet Engineering de-

274
275
276
277
278
279
280
281
282
283
284
285
286
287
288
289
290
291
292
293
294
295
296
297
298

scribed above, on the other hand, can be easily applied to a broad class of nonintegrable systems where FETH is expected to hold in certain regions. Long-range spin systems, in particular, where the exchange energies between far-off spins are taken into account in the model Hamiltonian, are good candidates because they are known to thermalize when driven with low frequencies [52].

II. LONG RANGE INTERACTIONS: THE LIPKIN MESHKOV GLICK MODEL:

The periodically driven Lipkin Meshkov Glick (LMG) model [20, 53] for N long-range spins is described by the Hamiltonian

$$\hat{H}(t) = \hat{H}_0 + [h \cos(\omega t) + h_0] \hat{H}_1. \quad (18)$$

Here, the undriven part \hat{H}_0 and the driven part \hat{H}_1 are, respectively,

$$\begin{aligned} \hat{H}_0 &= \frac{2}{N-1} \sum_{ij} \hat{\sigma}_i^z \hat{\sigma}_j^z, \\ \hat{H}_1 &= \sum_{i=1}^N \hat{\sigma}_i^x. \end{aligned} \quad (19)$$

The Kac-norm of $2/(N-1)$ arises from the choice to maintain the extensivity of the interaction energy. The Hamiltonian in equation 18 commutes with $P_{ij} \equiv \frac{1}{2}(1 + \vec{\sigma}_i \cdot \vec{\sigma}_j)$. In addition, it also commutes with the total angular momentum $S^2 = |\vec{S}|^2$, where $\vec{S} = S^x \hat{x} + S^y \hat{y} + S^z \hat{z} \equiv \frac{1}{2} \sum_i \vec{\sigma}_i$. We now choose to populate the system in a state with $S^2 = \frac{N}{2} \left(\frac{N}{2} + 1 \right)$. In that case, the dynamics remains invariant in the $N+1$ -dimensional space spanned by the common eigenstates of P_{ij} , $|S|^2$ and S_z ; the so-called *Totally Symmetric Subspace*, or TSS [54]. Let the eigenvalues

of S^z in the TSS be s_n , and the eigenvectors be $|s_n\rangle$. Here, $s_n = -\frac{1}{2} + \frac{n}{N}$ and the index $n = 0(1)N$ has $N+1$ values. The dynamics is restricted to this invariant subspace, wherein the matrix elements of the Hamiltonian are given by

$$\begin{aligned} \langle s_i | \hat{H}_0 | s_j \rangle &= -\frac{4}{N-1} s_i^2 \delta_{ij}, \\ \langle s_i | \hat{H}_1 | s_j \rangle &= \left[\sqrt{\frac{N}{2} \left(\frac{N}{2} + 1 \right)} - N s_i (N s_{i+1}) \delta_{i+1,j} \right. \\ &\quad \left. + \sqrt{\frac{N}{2} \left(\frac{N}{2} + 1 \right)} - N s_i (N s_{i-1}) \delta_{i-1,j} \right]. \end{aligned} \quad (20)$$

These allow for a numerical representation of the Hamiltonian in the TSS.

Next, we transform the Hamiltonian to the rotated frame given by the operator

$$\hat{U}(t) = \exp \left[i \frac{h}{\omega} \sin(\omega t) \hat{H}_1 \right]. \quad (21)$$

This is analogous to the rotation performed for the TFIM in eqns 10 and 11. Defining $\tau = \frac{h}{\omega} \sin \omega t$, we use the fact that $\hat{H}_1 = 2S^x$, as well as the following identity obtained by using the Baker-Campbell-Hausdorff formula,

$$e^{i2\tau \hat{S}^x} \hat{S}^z e^{-i2\tau \hat{S}^x} = \hat{S}^z \cos(2\tau) + \hat{S}^y \sin(2\tau), \quad (22)$$

to simplify the transformed Hamiltonian $\tilde{H}(t) = \hat{U}^\dagger(t) \hat{H}(t) \hat{U}(t) - \hat{U}^\dagger(t) \partial_t \hat{U}(t)$, yielding

$$\begin{aligned} \tilde{H}(t) &= -\frac{1}{N-1} \left[(S^z)^2 (1 + \cos 4\tau) + (S^y)^2 (1 - \cos 4\tau) \right. \\ &\quad \left. + \{S^y, S^z\} \sin 4\tau \right] - 2h_0 S^x. \end{aligned} \quad (23)$$

Next, we define $\eta \equiv 4h/\omega$ and use the Jacobi-Anger formula in eqn 12 to expand $\tilde{H}(t)$. This yields

$$\begin{aligned} \tilde{H}(t) &= -\frac{\hat{S}^2}{N-1} + \frac{(\hat{S}^x)^2}{N-1} - 2h_0 \hat{S}^x - \frac{J_0(\eta)}{N-1} \left[(\hat{S}^z)^2 - (\hat{S}^y)^2 \right] - \frac{2}{N-1} \left[(\hat{S}^z)^2 - (\hat{S}^y)^2 \right] \sum_{k=1}^{\infty} J_{2k}(\eta) \cos(2k\omega t) \\ &\quad - \frac{2}{N-1} \{ \hat{S}^y, \hat{S}^z \} \sum_{k=1}^{\infty} J_{2k-1}(\eta) \sin[(2k-1)\omega t]. \end{aligned} \quad (24)$$

If ω is large enough to smooth out the harmonic com-

ponents, we obtain the RWA,

$$\begin{aligned} \tilde{H}(t) &\approx \tilde{H}_{\text{RWA}} \equiv -\frac{\hat{S}^2}{N-1} + \frac{(\hat{S}^x)^2}{N-1} - 2h_0 \hat{S}^x \\ &\quad - \frac{J_0(\eta)}{N-1} \left[(\hat{S}^z)^2 - (\hat{S}^y)^2 \right]. \end{aligned} \quad (25)$$

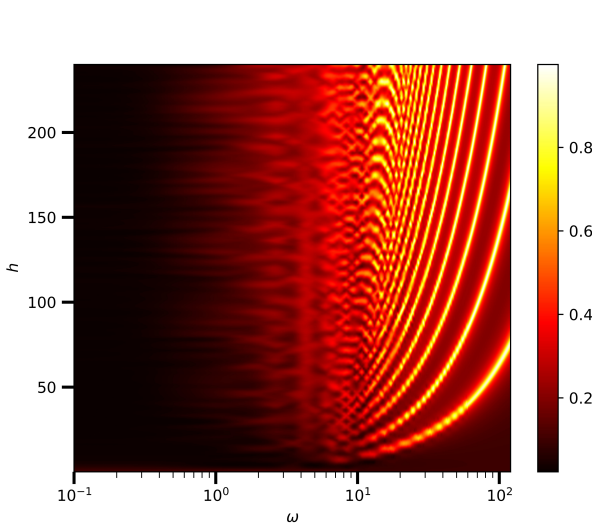


FIG. 3. Plot of the numerically averaged IPR (IPR computed using eqn 27) in the TSS plotted in the $h - \omega$ plane for $N = 100$ spins. In order to display the thermalized region more clearly, ω is plotted on a logarithmic scale on the abscissa. Note that, since the IPR is clearly non-negative, an average IPR of zero means that all Floquet states have zero IPR. Furthermore, the boundedness of IPR in $\phi_{IPR}(n) \leq 1$ ensures that if the average IPR is unity, then all Floquet states have unit IPR.

If the drive amplitude h is adjusted such that η lies at a root of $J_0(\eta)$ (the localization point), the RWA Hamiltonian is diagonal in the representation of the simultaneous eigenstates of transverse field \hat{S}^x , and S^2 , yielding an IPR of unity in that representation, similar to the TFIM in the previous section. Note however, that if the DC transverse field h_0 is set to 0, then, at the localization point, the RWA Hamiltonian $\tilde{H}_{\text{RWA}} \sim (\hat{S}^x)^2$ in the TSS. The eigenvalues are two-fold degenerate. This produces infinitely many (Floquet) eigenmodes in the degenerate subspace whose IPRs may not always be unity in the S^x representation. The removal of this degeneracy necessitates the inclusion of the d.c. field h_0 . However, note that rational values of h_0 may add accidental degeneracies in \tilde{H}_{RWA} . To see this, note that, at a localization point, the eigenvalues of \tilde{H}_{RWA} in the TSS are given by

$$\text{Eigs}\left[\tilde{H}_{\text{RWA}}\right] = \frac{\left(\frac{N}{2} - m\right)^2}{N-1} - 2h_0\left(\frac{N}{2} - m\right), \quad (26)$$

where the half-integer $-N/2 \leq m \leq N/2$ is the eigenvalue corresponding to a particular eigenstate $|m\rangle$ of the symmetry-breaking field \hat{S}^x . In order to ensure that no additional degeneracies occur, we have to set h_0 in such a way that no two energies accidentally coincide. If $N \gg 1$ (substantially large), then this condition can be readily met by assuring that $(1 - 2h_0)^{-1}$ is never an integer that is divisible by N . To ensure

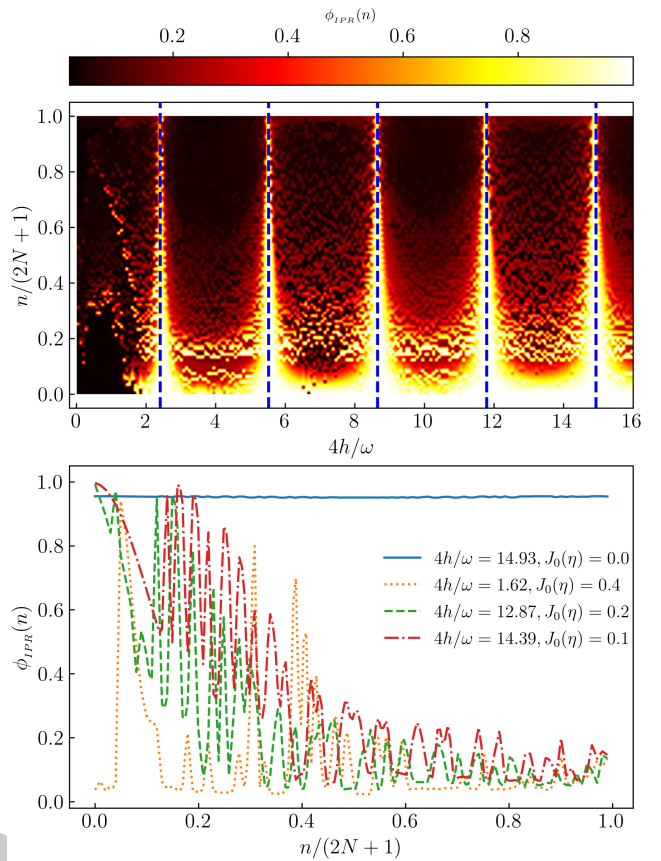


FIG. 4. IPR density plot for all possible Floquet modes (top panel ordinate) for different values of $\eta = 4h/\omega$ (top panel abscissa), deduced from equation 27 for exact LMG Hamiltonian for $N = 50$. Blue dashed lines are roots of $J_0(\eta)$. At bottom panel cross-section of IPR (ordinate) for four different η 's plotted for all possible floquet modes (bottom panel, abscissa) at $\omega = 90$. IPR founds to be \sim unity for all Floquet modes at roots of J_0 .

this in our numerical simulations, we have kept h_0 at a small irrational value. The localization of the Floquet states at resonance is supported by exact numerical results, as can be seen in the phase diagram fig 3. Here, we have plotted the arithmetic mean over all Floquet states of the IPR in the TSS for each point in the $h - \omega$ plane for $N = 100$ spins. The IPR in S^x representation is

$$\phi_{IPR}(n) = \sum_m |\langle m | \phi^n \rangle|^4. \quad (27)$$

As can be readily seen in the figure, the IPR is essentially zero when $\omega \lesssim 1$. There is considerable structure in the phase diagram for larger drive frequencies, and along the lines given by the roots of $J_0(\eta)$, the IPR is essentially unity, in agreement with eqn. 25.

In figure 4, we show plots of the IPR of the Floquet modes $|\phi^n\rangle$ for $S^2 = (N/2)(N/2 + 1)$. These plots were obtained numerically by diagonalizing the prop-

agator $U(t)$ at $t = T$, where $U(t)$ is defined in eqn 5. This propagator was obtained from simulations of the exact quantum dynamics using QuTiP, the Quantum Toolbox in Python [55]. We kept the frequency at a fairly large value $\omega = 90$ where we expect that RWA would be valid, and $N = \mathcal{O}(10^2)$. The density plot in the upper panel of fig 4 depicts the IPR of the Floquet states; the abscissa $\eta = 4h/\omega$ and the ordinate is $n/(2N + 1)$, where $n \leq 2N$ is a non-negative integer that indexes the Floquet states in increasing order of m . The dashed vertical lines correspond to the roots of $J_0(\eta)$. Comparing with the IPR of the TFIM in fig 1, we can see a very similar patterns in the immediate neighbourhood of the roots. Evidently, the IPR approaches a value of one for sufficiently large values of the roots, strongly suggesting full DMBL. Deviations occur at the smallest root of $J_0(\eta)$ (around $\eta = 2.405$) due to the contributions from higher order terms in eq 24. Thus, a higher root is favored for DMBL.

The bottom panel of fig 4 contains cross sections of the full IPR plot for selected values of η as indicated in the legend. When the drive amplitude h is adjusted such that η is close to a root of $J_0(\eta)$, the Floquet States are mixed, but not entirely thermal, since the IPR does not fall to $\mathcal{O}(N^{-1})$, indicating that localization persists to some extent. However, the further we are from the roots, the closer the IPR gets to one predicted by thermalization.

Figure 5 shows plots of the long-time average (from $t = 0 - 200T$) of the field amplitude $\langle \hat{S}^x \rangle$ as a function of η . The system is started from the fully polarized state $s_n = N/2$ in the TSS and the dynamics simulated. The average is plotted for different values of amplitude h , keeping the frequency fixed at a high value of $\omega = 90$. It is clearly very close to unity at roots of $J_0(\eta)$ and falls at points away from it, indicating that S^x is approximately conserved at the localization points.

Small deviations do occur due to the role of higher order terms in the rotated Hamiltonian in eq 23. This can be demonstrated quantitatively by comparing the IPR obtained from the exact dynamics simulation with that obtained from the dynamics of $\tilde{H}(t)$ in eq. 23 after truncating the series at orders $k \geq 1$. This comparison can be seen in fig 6. The IPR plots from the exact dynamics indicate that the first localization point, represented by the lowest root of $J_0(\eta)$, does not show complete DMBL. However, DMBL is particularly conspicuous at large roots. The IPRs of the Floquet states obtained from the RWA dynamics exhibit large deviations from unity when away from the localization point as evidenced by the green and red curves in the middle panel of fig 6. However, complete localization is seen in the RWA dynamics at any localization point, in contrast to the exact case in the top panel. Thus, it is necessary to incorporate higher-order corrections

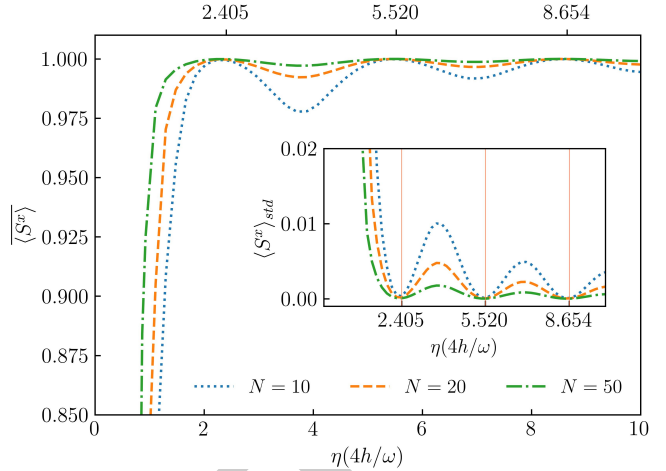


FIG. 5. Temporal average of $\langle \hat{S}^x \rangle$ (ordinate) for different η 's (abscissa) is plotted for $\sim 200T$ at higher ω for different $N=10, 20, 50$. $\langle \hat{S}^x \rangle$ is found to be unity at roots of $J_0(\eta)$. At points away from resonance points, $\langle \hat{S}^x \rangle$ falls below unity. The corresponding standard deviation $\langle \hat{S}^x \rangle_{std}$ supports the variation of $\langle \hat{S}^x \rangle$ (inset fig.). $\langle \hat{S}^x \rangle_{std}$ is ~ 0 describing a full freezing of the system at roots of $J_0(\eta)$ (red vertical solid lines).

into the Rotating Wave Approximation (RWA) at lower localization points. The application of the first-order correction to RWA in the lower panel of fig 6 results in a curve structure that is closer to that from the exact dynamics.

III. PERSISTENCE OF DMBL IN THE CONTINUUM LIMIT

In the continuum limit, where $N \rightarrow \infty$, the disparity between neighboring values of s_i in equation 20 can be disregarded, and s_i can be mapped to a continuum $q \in [-1/2, 1/2]$ [54]. We define the Hamiltonian per particle $h(t) \equiv \frac{H(t)}{N}$, and a canonically conjugate coordinate $Np \equiv \langle -i\frac{\partial}{\partial q} \rangle$. Then, in this limit, the dynamics can be approximated by that of a classical Hamiltonian [56]

$$h(t) = -2q^2 - [h \cos \omega t + h_0] \sqrt{1 - 4q^2} \cos p, \quad (28)$$

which yields the dynamical system

$$\begin{aligned} \frac{dq}{dt} &= \frac{\partial h}{\partial p} = h(t)\sqrt{1 - 4q^2} \sin p \\ \frac{dp}{dt} &= -\frac{\partial h}{\partial q} = 4q \left[1 - \frac{h(t) \cos p}{\sqrt{1 - 4q^2}} \right], \end{aligned} \quad (29)$$

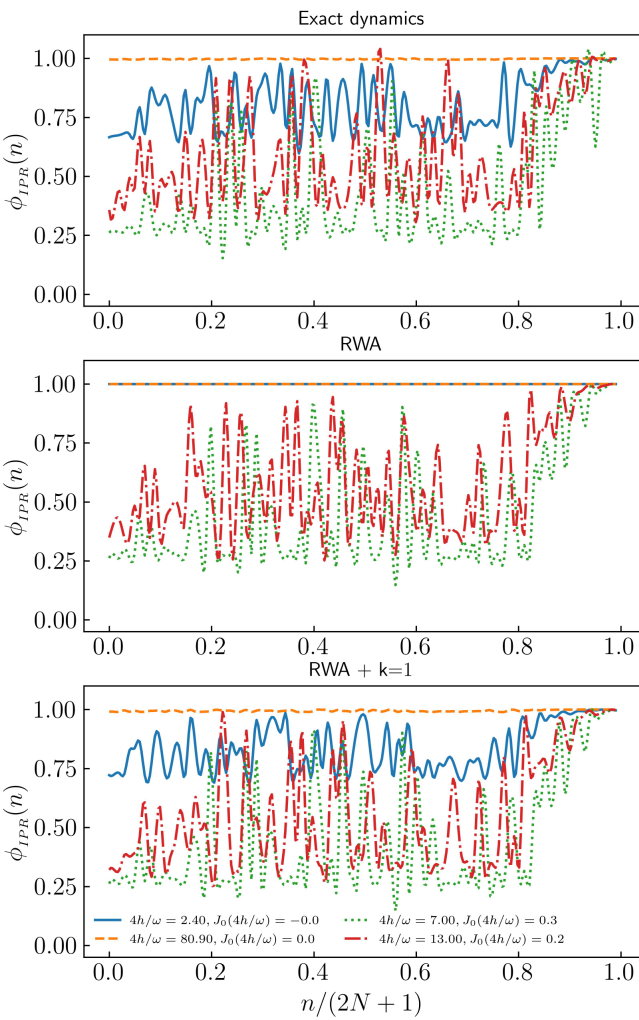


FIG. 6. The comparison between IPR for exact dynamics and RWA with corresponding correction orders. IPR is calculated for four different η 's and corresponding $J_0(\eta)$ values for colors, Blue: $\eta = 2.40, J_0(\eta) = 0.0$, dashed orange: $\eta = 80.9, J_0(\eta) = 0.0$, Green: $\eta = 7.0, J_0(\eta) = 0.3$, Red: $\eta = 13, J_0(\eta) = 0.2$. At low root of $J_0(\eta)$ IPR is not unity (Blue curve) where at higher root (orange dashed) it is unity while at points away from roots IPR are less than unity in the exact (top panel) plot. RWA does not matches with the exact plot. At all roots of $J_0(\eta)$ IPR is unity(middle panel). RWA with additional higher order terms exhibit similar system pattern(Bottom panel) with exact dynamics.

where $h(t) = [h \cos \omega t + h_0]$. We have profiled simulations of the ensuing dynamics with the Poincaré surface of section (PSOS) of the full dynamics. Here, the (q, p) -phase space is strobed at $t = nT$, and plotted

for a large number of initial conditions. The results are shown in the upper panels of fig 7 for a small value of $\omega = 2.0$ (left panel) and a large value $\omega = 90$ (right panel). In both cases, the value of h is chosen such that η lies on the first root of $J_0(\eta)$. The onset of chaos for small drive frequency indicates thermal behaviour for typical initial conditions, with small islands of regularity for others. This is consistent with similar results for small frequencies reported in [52, 57]. However, at high frequency, the regular islands distinctly dominate over the chaos. The trajectories indicate that the conservation of $\langle S^x \rangle \approx \sqrt{1 - 4q^2} \cos p$ [54] at high ω persists in the thermodynamic limit. That this is a signature of the underlying quantum dynamics can be readily seen in the quantum phase space representation of the Floquet Eigenstates for a large but finite N . These are shown in the corresponding lower panels of fig 7. Here, we have plotted the Spectral Average of the Husimi Q-functions of the acquired Floquet States in the TSS. Specifically, for a coherent state $|q, p\rangle$, the corresponding Spectral-Averaged Husimi distribution [58] is obtained by

$$H(q, p) \equiv \frac{1}{(2N+1)\pi} \sum_n \langle q, p | \phi^n \rangle \langle \phi^n | q, p \rangle. \quad (30)$$

The quantum phase space retains signatures of the classical phase space dynamics when $N = 100$, indicating the onset of the persistence of S^x conservation that arises from the resonance condition at high frequencies.

IV. PHASE CROSSOVER FROM THERMAL TO DMBL

The analysis of the periodically driven LMG model reveals two distinct scenarios at low and high external drive frequencies. In the former case, thermalization in accordance with FETH is seen, whereas in the latter case, DMBL is induced. As a result, we hypothesize that a macroscopic change in phase occurs due to the influence of frequency.

To demonstrate this, we investigate the IPR of the Floquet mode with smallest quasienergy for numerous frequencies and system sizes, along with the associated drive amplitude h keeping the system at a localization point. The results are shown in fig 8. In the low-frequency range $\omega \in [1.0, 9.0]$, the IPR exhibits values well below unity. Moreover, the IPR gradually diminishes with increasing system size, following a system size inverse proportional trend. Moreover, as can be seen in the bottom panel of the same figure, when the dynamics is simulated for smaller ωs , the fall of $\phi_{IPR}(N)$ asymptotically approaches one that characterizes a fully thermal state, where $\phi_{IPR}(N) \sim 1/N$ in the TSS. This confirms the participation distribution (as shown in the bottom panel). As In the limit

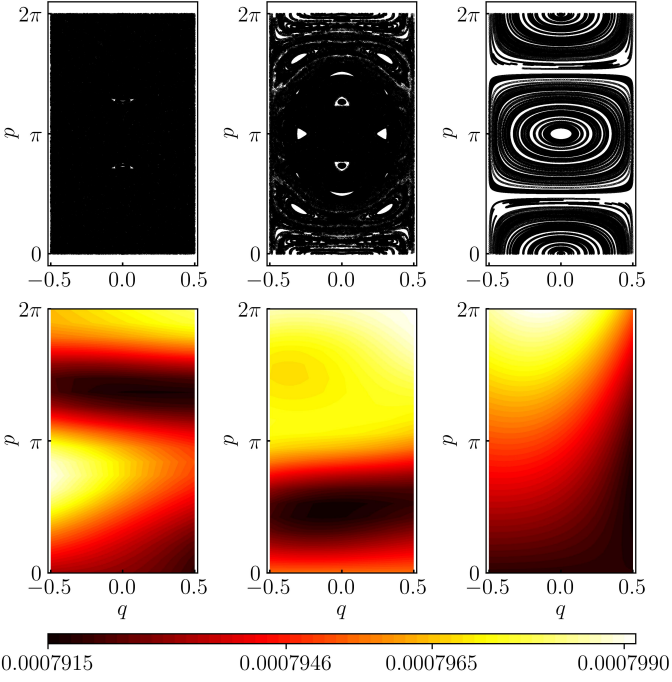


FIG. 7. Phase-space distributions at $\omega = 1.0$ (left panels), $\omega = 2.5$ (middle panels) and $\omega = 90.0$ (right panels) for 100 initial conditions. The drive amplitude h is always adjusted such that $\eta = 4h/\omega$ lies on the smallest root of $J_0(\eta)$, i.e. $\eta = 2.4048\dots$. At small $\omega = 1.0$, the classical PSOS, obtained from simulating the dynamics in eqns 29 (top left panel), shows chaotic behaviour, and at $\omega = 2.5$, regular regions start to appear. At higher $\omega = 90.0$, the dominance of regular dynamics can be readily seen (top right panel). The bottom panels plot the corresponding Spectral-Averaged Husimi-Q function, obtained from the Floquet modes $|\phi^n\rangle$ using eqn. 30, and setting $N = 100$. The $\omega = 1.0$ case (bottom left panel) has a dispersed distribution in colour. This is consistent with the chaotic behaviour seen in the continuum limit. At $\omega = 2.5$ (bottom middle panel), there is a partial regular pattern observed together with a dispersed pattern. In the $\omega = 90$ -case (bottom right panel), the distribution has distinct colour contrasts, which is consistent with the regular dynamics pattern seen in the continuum limit.

494 $N \rightarrow \infty$, the inverse participation ratio (IPR) tends to
495 towards zero, indicating a fully de-localized state. Con-
496 trast this with the IPR plots shown in the bottom left
497 panel of fig 2 for the integrable TFIM. The plots reveal
498 The top panel of fig. 8 also reveals a gradual increase
499 in the unity towards unity of IPR over a certain fre-
500 quency range, specifically at $\omega \approx 5$. In addition, the
501 rise does not cross with those for different values of
502 N , suggesting the onset of a phase crossover [42, 59].
503 As the size of the system increases, the crossover re-
506 gion becomes smoother, rather than sharper.

507 We can also look at this crossover more clearly in
508 the plots of the heating rate of the system, defined
509 simply by the expectation value of the Hamiltonian,

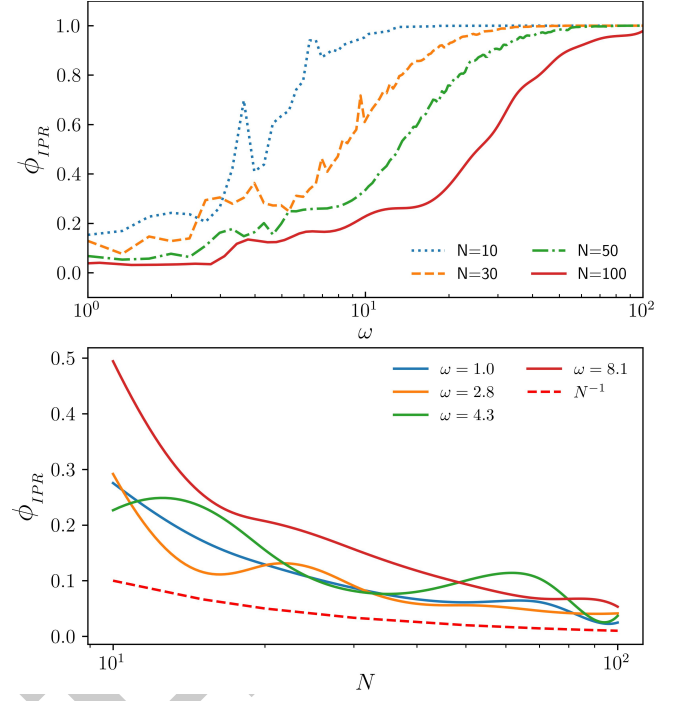


FIG. 8. In the top panel, the IPR of the lowest quasienergy Floquet state is plotted as a function of ω for different N s, with amplitude h adjusted to ensure that $J_0(\eta) = 0$ always. The smooth rise in IPR defines a phase crossover (top panel) between a fully thermal phase to a fully localized phase. The bottom panel plots the IPR versus N for small ω s, also with h adjusted. The curves asymptotically approach the dependency $\phi_{IPR} \sim 1/N$, indicating thermalization at low- ω .

510 $\langle \hat{H}(t) \rangle$. We have carried out the numerical eval-
511 uation from the simulated dynamics over $t = 500T$.
512 When the system is adequately described by FETH,
513 the temporal fluctuations in the Hamiltonian, defined
514 by $\langle H \rangle_{std}^2 \equiv \overline{\langle \hat{H} \rangle^2} - \overline{\langle \hat{H} \rangle}^2$ (see eqn 3), are minimal in
515 the thermodynamic limit, as the spread of states leads
516 to a limited standard deviation[60]. Conversely, the
517 onset of athermalities is indicated by nonzero fluctua-
518 tions in time. If we set the initial state to the fully po-
519 larized state in the TSS (given by $|s_N\rangle$), then the onset
520 of freezing, together with DMBL, will result in nearly
521 infinite hysteresis in the ensuing dynamics, causing
522 $|\psi\rangle(t) \approx |s_N\rangle \forall t$. From eqn. 18, we can clearly see
523 that this will lead to a linearly rising dependence on
524 ω in $\langle H \rangle_{std}$ as long as we stick to a localization point
525 given by a fixed h/ω [61]. All these observations are
526 corroborated by the heating rate plots in figure 9.

V. CONCLUSION AND OUTLOOK

We have delved into the onset of freezing and phase cross-over in 1D spin systems driven by a time-

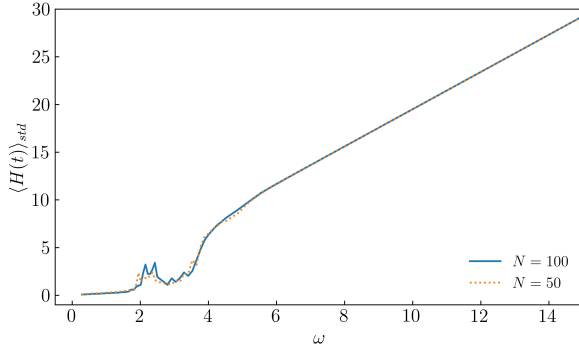


FIG. 9. The standard deviation of the heating rate, denoted by $\langle H \rangle_{std}$, calculated over a span of $t = 500T$ for two system sizes. Here, h is varied to keep $\eta = 4h/\omega$ at the first root of $J_0(\eta)$. A nonsingular rise has been identified at $\omega \approx 4.0$. $\langle H \rangle_{std}$ exhibits a diminutive magnitude below that value of ω , while a linear rise is observed at higher frequencies, consistent with freezing. A vanishingly small standard deviation for $\omega \ll 4.0$ indicates the presence of a thermal region, whereas a larger finite standard deviation suggests the existence of athermal behaviour. The small peaks observed at $\omega \in [2, 4]$ are finite-size effects that disappear in the thermodynamic limit.

530 periodic transverse field, contrasting the responses
 531 in the Transverse Field Ising Model (TFIM) with that
 532 of the long-range Lipkin-Meshkov-Glick Model (LMG).
 533 The parametrization of DMBL is based on the Inverse
 534 Participation Ratio (IPR) of the Floquet eigenstates.
 535 Our investigations compared the IPRs from both mod-
 536 els numerically, and found the emergence of thermal
 537 behavior at low frequencies and freezing at high fre-
 538 quencies for the LMG model, the latter a direct conse-
 539 quence of the appearance of additional approximately
 540 conserved quantities.

541 Long-range spins exhibit strong localization in spin-
 542 coordinate space for the LMG model when the drive
 543 frequency is $\omega \gg J$, where J represents the spin ex-
 544 change energy. The localization of the LMG model
 545 occurs at specific resonance points of the drive fre-
 546 quency ω and amplitude h , at $J_0(4h/\omega) = 0$, $\omega \gg J$.
 547 This is apparently similar to the phenomenon of Dy-
 548 namical Freezing (DMF) in the Transverse Field Ising

549 Model (TFIM), where comparable localization at res-
 550 onance points, determined by the roots of $J_0(2h/\omega)$,
 551 occurs due to the onset of an additional approximate
 552 conservation in the transverse field itself. However,
 553 a key difference is the thermal behaviour of the LMG
 554 model at low frequencies. Plots of the IPR for a range
 555 of frequencies along the resonance manifold exhibits
 556 a smooth increase in IPR yielding a quantum phase-
 557 crossover from a thermal phase governed by the Flo-
 558 quet Eigenstate Thermalization Hypothesis (FETH) to
 559 a Dynamically Many-Body localized phase (DMBL).
 560 This crossover is absent in the TFIM, as can be readily
 561 seen in the significant magnitude of the inverse par-
 562 ticipation ratio (IPR) even at low frequencies. Thus,
 563 the suppression of thermalization through Dynamical
 564 Many Body Localization in long-range systems can be
 565 controlled via Floquet engineering, even in clean sys-
 566 tems without any disorder. Thus, periodically driven
 567 long-range spin systems are an excellent tool for in-
 568 vestigating disorder-free Many Body Localization, as
 569 can be readily seen via the IPR of its Floquet modes.

570 There are several unexplored indicators of DMBL,
 571 such as entanglement entropy and level statistics [10],
 572 which we defer to future studies. In addition,
 573 Halpern in 2019 proposed a quantum engine based
 574 on MBL[11] which works between strong localized
 575 and thermal phases of the system. In our proposed
 576 LMG model, tuning the system parameters by bring-
 577 ing them to the resonance points, then adiabatically
 578 cycling the frequency from the thermal region to the
 579 DMBL region, can achieve a similar engine without
 580 going through a phase transition.

A. Acknowledgements:

581 One of the authors, MR acknowledges The Univer-
 582 sity of Burdwan for support via a state-funded fel-
 583 lowship. AR acknowledges support from the Uni-
 584 versity Grants Commission (UGC) of India, via BSR
 585 Startup Grant No. F.30-425/2018(BSR), as well as
 586 from the Science and Engineering Research Board
 587 (SERB) Core Research Grant No. CRG/2018/004002.

-
- 589 [1] P. Bordia, H. Lüschen, U. Schneider, M. Knap, and 596 [5] H. S. Yamada and K. S. Ikeda, Phys. Rev. E **105**, 054201
 590 I. Bloch, Nature Physics **13**, 460 (2017). 597 (2022).
 591 [2] S. Sahoo, I. Schneider, and S. Eggert, (2019), 598 [6] A. Roy and A. Das, Phys. Rev. B **91**, 121106 (2015).
 592 arXiv:1906.00004 [cond-mat.str-el]. 599 [7] H. Li, B. Shapiro, and T. Kottos, Phys. Rev. B **98**,
 593 [3] A. Das, Phys. Rev. B **82**, 172402 (2010). 600 121101 (2018).
 594 [4] G. B. Mbeng, A. Russomanno, and G. E. Santoro, 601 [8] A. Eckardt and E. Anisimovas, New Journal of Physics
 595 (2020), arXiv:2009.09208 [quant-ph]. 602 **17**, 093039 (2015).

- 603 [9] L. Zhang, V. Khemani, and D. A. Huse, Phys. Rev. B **94**, 659 [38] M. Vogl, M. Rodriguez-Vega, and G. A. Fiete, Phys. Rev. 604 224202 (2016). 660 B **101**, 024303 (2020).
- 605 [10] V. Khemani, A. Lazarides, R. Moessner, and S. L. 661 [39] M. Bukov, L. D'Alessio, and A. Polkovnikov, Advances in 606 Sondhi, Phys. Rev. Lett. **116**, 250401 (2016). 662 Physics **64**, 139 (2015).
- 607 [11] N. Yunger Halpern, C. D. White, S. Gopalakrishnan, and 663 [40] L. D'Alessio and M. Rigol, Phys. Rev. X **4**, 041048 608 G. Refael, Phys. Rev. B **99**, 024203 (2019). 664 (2014).
- 609 [12] T. Nag, S. Roy, A. Dutta, and D. Sen, Phys. Rev. B **89**, 665 [41] R. Yousefjani, S. Bose, and A. Bayat, Phys. Rev. Res. **5**, 610 165425 (2014). 666 013094 (2023).
- 611 [13] G. Carleo, F. Becca, M. Schiró, and M. Fabrizio, Scien- 667 [42] P. Sierant, M. Lewenstein, A. Scardicchio, and J. Za- 612 tific Reports **2**, 243 (2012). 668 krzewski, Phys. Rev. B **107**, 115132 (2023).
- 613 [14] S. Aditya and D. Sen, (2023), arXiv:2305.06056 [cond- 669 [43] F. Alet and N. Laflorencie, Comptes Rendus Physique 614 mat.stat-mech]. 670 **19**, 498 (2018).
- 615 [15] M. Schiulaz, A. Silva, and M. Müller, Phys. Rev. B **91**, 671 [44] S. J. Garratt and S. Roy, Phys. Rev. B **106**, 054309 616 184202 (2015). 672 (2022).
- 617 [16] T. Grover and M. P. A. Fisher, Journal of Statistical Me- 673 [45] R. B. Stinchcombe, Journal of Physics C: Solid State 618 chanics: Theory and Experiment **2014**, P10010 (2014). 674 Physics **6**, 2459 (1973).
- 619 [17] Z. Papić, E. M. Stoudenmire, and D. A. Abanin, Annals 675 [46] F. E. H. George Arfken, Hans Weber, *Mathematical 620 of Physics* **362**, 714 (2015). 676 Methods for Physicists, 7th ed. (Academic Press, 2011).
- 621 [18] A. Smith, J. Knolle, D. L. Kovrizhin, and R. Moessner, 677 [47] S. Mukherjee, A. Spracklen, D. Choudhury, N. Gold- 622 Phys. Rev. Lett. **118**, 266601 (2017). 678 man, P. Öhberg, E. Andersson, and R. R. Thomson, New 623 [19] O. Hart, S. Gopalakrishnan, and C. Castelnovo, Phys. 679 Journal of Physics **17**, 115002 (2015). 624 Rev. Lett. **126**, 227202 (2021).
- 625 [20] H. Lipkin, N. Meshkov, and A. Glick, Nuclear Physics 680 [48] S.-H. Lin, B. Sbierski, F. Dorfner, C. Karrasch, and 626 **62**, 188 (1965). 681 F. Heidrich-Meisner, SciPost Phys. **4**, 002 (2018).
- 627 [21] N. Meshkov, A. Glick, and H. Lipkin, Nuclear Physics 682 [49] N. C. Murphy, R. Wortis, and W. A. Atkinson, Phys. Rev. 628 **62**, 199 (1965). 683 B **83**, 184206 (2011).
- 629 [22] A. Glick, H. Lipkin, and N. Meshkov, Nuclear Physics 684 [50] E. J. Torres-Herrera, I. Vallejo-Fabila, A. J. Martínez- 630 **62**, 211 (1965). 685 Mendoza, and L. F. Santos, Phys. Rev. E **102**, 062126 631 [23] P. Ribeiro, J. Vidal, and R. Mosseri, Phys. Rev. E **78**, 686 (2020).
- 632 021106 (2008). 687 [51] N. Trivedi and D. Heidarian, Progress of Theoretical 633 [24] N. Debergh and F. Stancu, Journal of Physics A: Math- 688 Physics Supplement **160**, 296 (2005).
- 634 ematical and General **34**, 3265 (2001). 689 [52] A. Russomanno, R. Fazio, and G. E. Santoro, Euro- 635 [25] P. Titum and M. F. Maghrebi, Phys. Rev. Lett. **125**, 690 physics Letters **110**, 37005 (2015).
- 636 040602 (2020). 691 [53] N. Defenu, T. Enss, M. Kastner, and G. Morigi, Phys. 637 [26] A. Campa, T. Dauxois, and S. Ruffo, Physics Reports 692 Rev. Lett. **121**, 240403 (2018).
- 638 **480**, 57 (2009). 693 [54] T. Mori, Journal of Physics A: Mathematical and The- 639 [27] T. Eisele and R. S. Ellis, Journal of Statistical Physics 694 oretical **52**, 054001 (2019).
- 640 **52**, 161 (1988). 695 [55] J. Johansson, P. Nation, and F. Nori, Computer Physics 641 [28] A. Canning, Physica A: Statistical Mechanics and its 696 Communications **184**, 1234 (2013).
- 642 Applications **185**, 254 (1992). 697 [56] B. Sciolla and G. Biroli, Phys. Rev. Lett. **105**, 220401 643 [29] D. Vu, K. Huang, X. Li, and S. Das Sarma, Phys. Rev. 698 (2010).
- 644 Lett. **128**, 146601 (2022). 699 [57] R. A. Kidd, M. K. Olsen, and J. F. Corney, Phys. Rev. A 700 [58] A. Bäcker, S. Fürstberger, and R. Schubert, Phys. Rev. 645 [30] G. Misguich, V. Pasquier, and J.-M. Luck, Phys. Rev. B 701 **100**, 013625 (2019).
- 646 **94**, 155110 (2016). 702 [59] S. Sachdev, *Quantum Phase Transitions*, 2nd ed. (Cam- 647 [31] M. Calixto and E. Romera, Journal of Statistical Me- 703 bridge University Press, Cambridge, 2011).
- 648 chanics: Theory and Experiment **2015**, P06029 (2015). 704 [60] P. Reimann, Journal of Statistical Mechanics: Theory 649 [32] K. Fujii, Journal of Modern Physics **8**, 2042 (2017). 705 and Experiment **2021**, 103106 (2021).
- 650 [33] B. Sutherland, *Beautiful Models* (WORLD SCIENTIFIC, 651 2004) Chap. 2.
- 652 [34] D. A. Abanin, E. Altman, I. Bloch, and M. Serbyn, Rev. 706 [61] When frozen, $|\psi(t)\rangle \approx |s_N\rangle$. From eqn 18, $\langle \hat{H}_{0,1} \rangle$ 653 Mod. Phys. **91**, 021001 (2019). 707 are both approximately constant. Averaging the square of 654 [35] M. Srednicki, Phys. Rev. E **50**, 888 (1994). 708 $\langle \hat{H}(t) \rangle$ over long times $\tau \gg T$ yields a result that goes 655 [36] M. Srednicki, Journal of Physics A: Mathematical and 709 as $h^2 + \delta$, where $\delta \sim h_0 \ll 1$. Thus, the standard devia- 656 General **32**, 1163 (1999). 710 tion in time will go as $\sim h \sim \omega$, since $\eta = 4h/\omega$ is kept 657 [37] M. Holthaus, Journal of Physics B: Atomic, Molecular 711 fixed.
- 658 and Optical Physics **49**, 013001 (2015). 712